Journal of
Nanoelectronics and Optoelectronics
Vol. 8, 397–414, 2013

REVIEW

Magnetism of Iron Oxide Nanoparticles and Magnetic Biodetection

L. Li[1], C. W. Leung[2], and P. W. T. Pong[1,*]

[1] Department of Electrical and Electronic Engineering, The University of Hong Kong, Hong Kong
[2] Department of Applied Physics, Hong Kong Polytechnic University, Hong Kong

Magnetic biodetection systems based on the magnetic properties of nanoparticles have received considerable attention because most biological samples exhibit no magnetic background and highly sensitive measurements can be performed in visually obscured biological samples. Magnetic iron oxide nanoparticles (IONPs) emerge as an excellent candidate because they are physically and chemically stable, bio-compatible, environmentally safe, and inexpensive to produce. This review focuses on the IONP-based magnetic biodetection and how the magnetic properties of IONPs are used to determine the presence of the bound bioanalytes. The magnetic permeability, magnetic relaxation, and stray magnetic field of IONPs are elaborated and the mechanism they are being applied in magnetic biodetection is explained. Information about the typical chemical synthesis methods and the properties of the IONP products are summarized. Recent advances on the magnetic biodetection with IONPs are explored. Moreover, the prospect of using IONP-based magnetic biodetection to provide a multiplexing and miniaturized testing platform for health care is revealed.

Keywords: Magnetic Biodetection, Iron Oxide Nanoparticles, Magnetic Relaxation, Magnetic Susceptibility, Stray Magnetic Field.

CONTENTS

1. INTRODUCTION

A highly sensitive and rapid quantitative biodetection system is very important for early medical diagnosis as well as in molecular biology research area.[1,2] The fluoroimmunoassay is widely used in biodetection technologies.[3–7] However, this method is susceptible to external interference, such as the fluorescent background of biological components, fluorescence quenching and photobleaching of the fluorescent probes. The biodetection method utilizing magnetic nanoparticles and magnetic sensors as bio-labels and detectors is remarkably advantageous over the traditional means.[8–10] The dimension of magnetic nanoparticles is compatible with biological targets such as protein with size of few nanometers. The small size of magnetic nanoparticles avoids blocking biomolecular interactions, and one small nanoparticle tends to conjugate with one biomolecule or at most a few of them, which allows establishing a quantitative relation between the number of captured particles and the amount of actual biological molecules.[11] The magnetic properties of magnetic nanoparticles are very stable, and they are not subject to photo-bleaching. Most biological systems do not exhibit significant magnetic background, thus the magnetic signal of magnetic nanoparticles can be detected with high signal-to-noise ratio. In addition, magnetic nanoparticles can be remotely manipulated by applying a magnetic field.

Magnetic nanoparticles used as bio-probes are essential for a successful magnetic biodetection, and iron oxide

*Author to whom correspondence should be addressed.

nanoparticles (IONPs) have been a popular choice due to their high physical and chemical stability, low toxicity, environmentally safe property, and inexpensive production cost. The composition, size, and magnetic property of the IONPs can be modulated through synthesis process. The magnetic signals of IONPs can be detected by using advanced and newly developed instruments of microelectronics, spintronics, and nanotechnologies. This review is divided into three sections. The first section provides an overview of the fundamental magnetic properties of IONPs which are (i) magnetic permeability, (ii) magnetic relaxation, and (iii) stray magnetic field, and the biosensing principles that employ these properties are also mentioned. The typical and representative synthesis methods of IONPs and the properties of the corresponding end-products are described in the second section. The last section reviews the recent research developments in the IONP-based magnetic detection configurations. The prospect of using IONP-based magnetic biodetection with appropriate magnetic signal detectors, to provide a multiplexing and miniaturized testing platform for health care application, is also revealed.

2. MAGNETISM OF IONPs

2.1. Magnetic Relaxation of IONPs

As the applied magnetic field is changed, IONPs show magnetic relaxation behavior and reach to an equilibrium or steady-state condition. The characteristic time in magnetic relaxation is known as relaxation time, which is influenced by both the environment and the properties of the particle itself. Thus, the investigation of magnetic relaxation can give information about the size and status (mobile or immobile) of the particle. Magnetorelaxometry is the measurement of the relaxation of magnetic particles. In a typical magnetorelaxometry for IONPs, the moments of magnetic nanoparticle are first aligned by a magnetic field and the net magnetic signal decay as a function of time is detected after removing the field.[12, 13] Generally speaking, the magnetic relaxations of IONPs fall into two categories: Neel relaxation and Brownian relaxation (Fig. 1).

L. Li received the B.S. degree from Shanghai Jiao Tong University in 2006, the M.S. degree from Fudan University in 2009, and the Ph.D. degree from the University of Hong Kong (HKU) in 2013. Currently, she is a Post-doctoral Fellow in the Department of Electrical and Electronic Engineering, HKU, working on the biosensing platform utilizing magnetic nanoparticles and magnetoresistive sensors.

C. W. Leung received the Ph.D. degree in Department of Material Science from the University of Cambridge, Cambridge, U.K., in 2002. He was a Croucher Foundation Research Fellow in the University of Cambridge for three years. In 2005, he joined the Department of Applied Physics, Hong Kong Polytechnic University, as a lecturer. Currently, he is an assistant professor in Hong Kong Polytechnic University, working on spintronics, nanofabrication techniques, and organic thin film devices.

P. W. T. Pong received the Ph.D. degree in engineering from the University of Cambridge in 2005. He was a Postdoctoral Researcher at the Magnetic Materials Group, National Institute of Standards and Technology (NIST), Gaithersburg, MD, USA, for three years. In 2008, he joined the Faculty of Engineering, the University of Hong Kong, as an Assistant Professor, working on tunneling magnetoresistance (TMR) sensors, and the application of magnetoresistive sensors in biomedical area and Smart Grid.

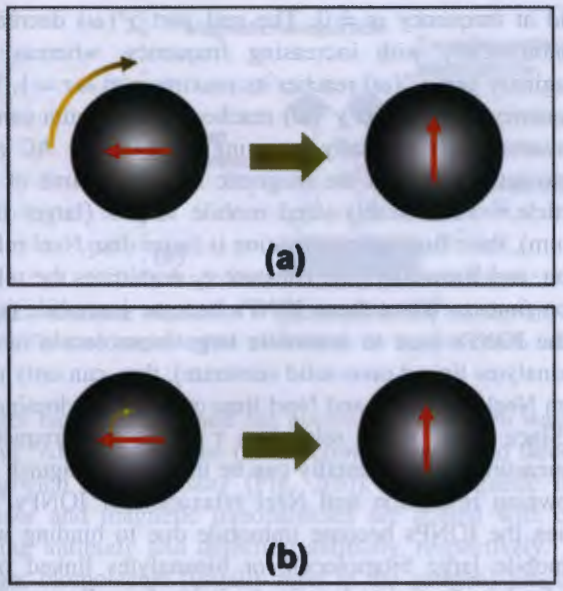

Fig. 1. Relaxation mechanism of a single-domain iron oxide nanoparticle (IONP). (a) Brownian relaxation, the yellow arrow represents the physical rotation of the entire IONP. (b) Neel relaxation, the dashed yellow arrow represents the rotation of magnetic moment within the IONP. The red arrow represents the direction of magnetization.

For mobile IONPs, both the Brownian relaxation and Neel relaxation exist after an applied magnetic field is removed. For immobile IONPs, only Neel relaxation exists after removing the magnetic field. As shown in Figure 1(a), the Brownian relaxation is the physical rotation of the IONPs with relaxation time (τ_B), which is mainly determined by the hydrodyanmic sizes of the IONPs in ferrofluid, viscosity of the medium, and temperature. The Brownian relaxation time can be found by: $\tau_B = 3\eta V_H/k_BT$, where η is the viscosity of the medium, V_H is the hydrodynamic volume, k_B is Boltzmann's constant and T is the temperature. As shown in Figure 1(b), the Neel relaxation is the rotation of the magnetic moments within the IONPs with relaxation time (τ_N), which originates from the anisotropy of the crystalline lattice.[14] When the IONP is magnetized along the easy magnetization axis, the energy is minimized. If the external field rotates the magnetization away from the easy axis, the magnetization eventually returns to its preferred direction after the external field is removed. The Neel relaxation time for a single domain particle is independent of the hydrodynamic size of the particle, and it can be found by: $\tau_N = \tau_0 \exp(\Delta E/k_BT)$, where τ_0 is the order of 10^{-10}–10^{-12} s, k_BT is the thermal energy, and ΔE is the energy barrier to moment reversal. In the simplest cases, it is given by $\Delta E = KV$, where K is the magnetic anisotropy constant and V is the magnetic core volume. The parameters τ_0 and K depend on the shape of the particle. The effective relaxation time (τ_{eff}) for the mobile particles can be derived by considering both Brownian and Neel relaxation act simultaneously: $1/\tau_{\text{eff}} = 1/\tau_B + 1/\tau_N$. The equation of τ_{eff} indicates that the smallest time constant dominates the physical process of particle relaxation, which is related to the hydrodynamic size and magnetic core volume. Generally speaking, Neel relaxation is faster than Brownian relaxation for small particles, while the Brownian relaxation is faster than Neel relaxation for large particles. There usually exists a critical volume above which the Brownian relaxation mechanism becomes dominant ($\tau_N \gg \tau_B$), in which the Brownian time constant τ_B dominates τ_{eff}; for an ideal single-domain spherical IONP at room temperature, the typical critical diameter is about 20 nm.[15]

By utilizing suitably sized IONPs on which Brownian relaxation is much faster than Neel relaxation,[16] there are mainly three kinds of biodetection mechanisms which can be realized through magnetometry. In the first mechanism, there is no crosslink during the detection of small biomolecules. When the small biomolecules bind onto the surface of a mobile IONP in suspension, the IONP remains mobile but with an increased hydrodynamic size. The increased hydrodynamic size of IONPs after binding with small biomolecules results in an increased Brownian relaxation time while Neel relaxation time remains unchanged. Thus the biomolecule-bound IONPs can then be distinguished from the unbound ones by their increased Brownian relaxation time. In the second mechanism, the detection of biomolecules takes place through the crosslinking process whereby IONPs forming clusters. When the concentration of detecting biomolecules increases, larger size of IONP-biomolecule clusters form during the crosslinking process and the Brownian relaxation time of the magnetic clusters increases accordingly. When these clusters become large enough, the Brownian relaxation becomes so slow that the relaxation is dominated by the Neel mechanism, where the maximum relaxation time constant is reached. Therefore, before the Neel mechanism dominates the relaxation, the concentration of detecting biomolecules can be obtained from the relaxation time of magnetic clusters. The third mechanism is about the detection of large immobile biomolecules in suspension or bioanalytes attached onto a solid substrate. When the IONPs bind to the immobile large biomolecule or bioanalytes linked onto solid substrate, the IONPs are immobilized into immobile status and their relaxation switches from Brownian to Neel relaxation. On the other hand, the unbound IONPs are still dominated by the Brownian relaxation. Thus, the biomolecule-bound IONPs can be distinguished from the unbound ones by their different relaxation times.[17]

2.2. Magnetic Permeability (Susceptibility) of IONPs

The magnetic permeability/susceptibility indicates the ability of an IONP to become magnetized in response to an applied magnetic field. In magnetic biodetection, both magnetic permeability and magnetic susceptibility have been used in literature and they are closely related to each other. When a magnetic field (H) is applied, atomic

REVIEW

moments of individual particle contribute to the overall magnetic induction B: $\mathbf{B} = \mu_0(\mathbf{H}+\mathbf{M}) = \mu_0(1+\chi)\mathbf{H} = \mu_0\mu_r\mathbf{H} = \mu\mathbf{H}$, where μ_0 is the permeability of free space, μ_r is relative magnetic permeability, μ is magnetic permeability, and the magnetization $\mathbf{M}$ is the magnetic moment on a volume $\mathbf{V}$ of the particle (magnetic dipole moment per unit volume). The volumetric magnetic susceptibility, χ, describes the relation between the magnetic field $\mathbf{H}$ and the magnetization $\mathbf{M}$ induced in particles by the magnetic field: $\mathbf{M} = \chi\mathbf{H}$. Thus, the volumetric magnetic susceptibility χ, and the magnetic permeability μ, are related by the following formula: $\mu = \mu_0(1+\chi)$, while the magnetic susceptibility and the relative permeability are related as: $\mu_r = 1+\chi$.

There are two main kinds of biodetection schemes which utilize the magnetic permeability/susceptibility of IONPs. The first one is based on the measurement of magnetic permeability by using inductance-based magnetic permeability detector. For a given material, the relative magnetic permeability (μ_r) is a constant value. When a magnetic material is placed inside a coil, the inductance L for the coil is described by $L = (\mu_r\mu_0 A)/lN^2$, where μ_r is the relative magnetic permeability of the material in the coil, μ_0 is the permeability of a vacuum, A is the cross-section area of the coil, l is the coil length and N is the turn number of the coil. Thus, the signal of IONPs can be measured by placing them into the magnetic permeability detector. Based on this principle, the first biosensor utilizing magnetic permeability was developed by Kriz et al. in 1996.[18] In this kind of detection scheme, superparamagnetic iron oxide nanoparticles (SPIONs) is preferable. This is because SPIONs with size less than 10 nm usually consist of single magnetic domains,[19] and all of the magnetic domains can be aligned in SPIONs. In large magnetic nanoparticles, they typically consist of multiple magnetic domains that are not well aligned and thus interfere with each other.[20] Therefore, SPIONs exhibit a relative high magnetic permeability/susceptibility which can induce stronger output signal in the inductive coil.

The second scheme of detection is based on the magnetic complex susceptibility of IONPs, which is closely related to the relaxation mechanism of IONPs. Due to the finite rate of magnetization change with time, the magnetization of ferrofluid lags behind the application of a magnetic field. In this case, the dynamic behavior of magnetized ferrofluid in response to an alternating magnetic field can be described by the complex magnetic susceptibility, $\chi(\omega) = \chi'(\omega) - i\chi''(\omega)$. The in-plane component of the magnetic susceptibility $\chi'(\omega)$, is related to the storage of the magnetic energy; while the quadrature component $\chi''(\omega)$, is related to the dissipation of magnetic energy. According to Debye's theory,[21] the spectrum of the complex magnetic susceptibility of the fluid is given by: $\chi'(\omega) = \chi_0/[1+(\omega\tau)^2]$, $\chi''(\omega) = \chi_0\omega\tau/[1+(\omega\tau)^2]$, where χ_0 is the magnetic susceptibility of the fluid at frequency $\omega = 0$. The real part $\chi'(\omega)$ decreases monotonically with increasing frequency, whereas the imaginary part $\chi''(\omega)$ reaches its maximum at $\omega\tau = 1$. The frequency ω at which $\chi''(\omega)$ reaches its maximum can be measured experimentally by using for example AC susceptometer, and τ is the magnetic relaxation time of the particle.[22] For suitably-sized mobile IONPs (larger than 20 nm), their Brownian relaxation is faster than Neel relaxation, and Brownian time constant τ_B dominates the relaxation time τ. When these IONPs become immobile (e.g., if the IONPs bind to immobile large biomolecule or the bioanalytes linked onto solid substrate), they can only perform Neel relaxation and Neel time constant τ_N dominates τ. Since τ and ω are related as $\tau = 1/\omega$, the frequency ω measured experimentally can be used to distinguish the Brownian relaxation and Neel relaxation of IONPs.[10, 23] When the IONPs become immobile due to binding with immobile large biomolecule or bioanalytes linked onto solid substrate, their relaxation switches from Brownian to Neel relaxation. On the other hand, the unbound IONPs maintain the Brownian relaxation. Thus, the bound IONPs can be distinguished from the unbounded ones by their frequency ω at which $\chi''(\omega)$ reaches its maximum.

When biomolecule is bound to a magnetic particle, there is an increase in hydrodynamic radius of the particle. For the mobile IONP dominated by Brownian relaxation, its Brownian relaxation time τ_B satisfies the equation $\tau_B = 3\eta V/k_B T$ as discussed previously, which is related to its particle hydrodynamic size. Since the frequency ω at which $\chi''(\omega)$ reaches its maximum has relation with τ_B as $\omega\tau_B = 1$, ω is also related to the particle hydrodynamic size. Thus, the increase of the hydrodynamic radius of the particle after binding with biomolecules is reflected by the decrease of frequency ω of the maximum $\chi''(\omega)$. From the frequency dependence of complex susceptibility $\chi''(\omega)$, the biomolecule-bound IONPs can be distinguished from the unbound IONPs.

2.3. Stray Magnetic Field of IONPs

Detection based on the change of magnetic relaxation or magnetic permeability/susceptibility works in substrate-free schemes. Therefore, when the biodetection is carried out with the presence of a substrate, the measurement of stray magnetic field of IONPs is usually performed instead.[24] As shown in Figure 2, two common kinds of bioassays have been carried out by using magnetic field sensors and magnetic nanoparticles. The biodetection can be carried out through complementary connection between two biomolecules (e.g., streptavidin-biotin interaction or complementary DNA sequence recognition) (Fig. 2(a)). The target biomolecules are immobilized on the surface of magnetic field sensor, and the complementary biomolecules are coated onto the magnetic nanoparticles. When the bio-labeled magnetic nanoparticles pass over the sensor surface, they are bound to the

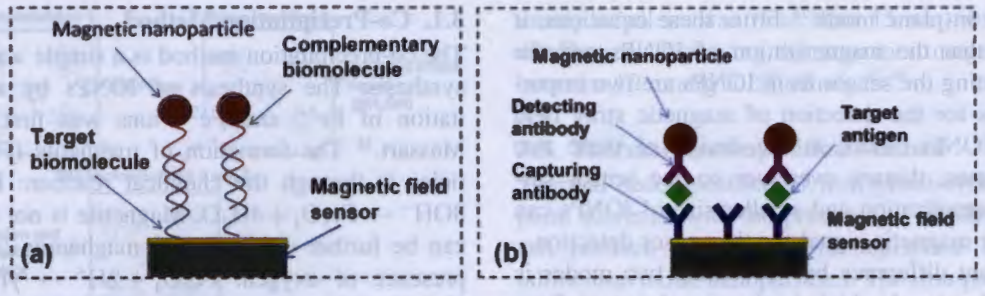

Fig. 2. Schematic illustrations of (a) complementary bioassay and (b) sandwich immunoassay based on magnetic field sensor and magnetic nanoparticles. The stray magnetic field produced by the magnetic labels induces a signal in the magnetic field sensor.

target biomolecules, and the excess ones are then washed away. Alternatively, the biodetection is conducted through sandwich immunoassay (Fig. 2(b)). The magnetic field sensor and magnetic nanoparticles are coated with capturing antibody and detecting antibody, respectively. The target biomolecule (usually refer to the antigen) acts as a linker between the magnetic nanoparticles and magnetic field sensor, and the excess magnetic nanoparticles are then washed away. Finally, the magnetic stray field from the bound magnetic nanoparticles is detected by the magnetic field sensor, which reflects the presence of the target bioanalytes.

The stray field is the magnetic field generated by the magnetization in a magnetic particle. To acquire ultrahigh sensitivity in biodetection by using magnetic field biosensors, the IONPs need to possess high magnetic moment so that the stray magnetic field generated can be strong enough to be detected by the magnetic field sensor. In addition, the IONPs also need to be superparamagnetic so that particle agglomeration can be avoided when there is no applied magnetic field.[25] However, the superparamagnetic IONPs have to be magnetized by an excitation magnetic field in order to produce a stray field as sensor signal. There are two major directions to apply the excitation magnetic field: vertical mode and in-plane mode. As shown in Figure 3, it is assumed that the origin $(0, 0, 0)$ is located at the center point of the particle. The sensitive direction of the sensor is along the x-direction, thus only the magnetic stray field along the x-direction emanated from the IONPs can be detected by the sensor. In the vertical mode (Fig. 3(a)), an external magnetic field is applied along the direction perpendicular to the sensor surface (z direction). The magnetic stray field along the x-direction produced by a single magnetic particle is related to its magnetic moment, and is given by $B_x = \mu_0 3mzx/(4\pi(x^2+y^2+z^2)^{5/2})$ where m is the magnetic moment of the particle. In the in-plane mode (Fig. 3(b)), an external magnetic field is applied along the direction parallel to the sensor surface (x direction). The magnetic stray field along the x-direction produced by a single magnetic particle is also related to its magnetic moment, and is given by $B_x = (\mu_0 m/4\pi(x^2+y^2+z^2)^{3/2})(3x^2/(x^2+y^2+z^2)^{5/3}-1)$. If the magnetic particle with radius a is separated from a sensor by an overlayer with thickness t, by substituting $z = (a+t)$, $d = (x^2+y^2)^{1/2}$ and $m = 4M\pi a^3/3$ where M is the magnetization of the particle (magnetic dipole moment per unit volume), the stray magnetic field emanated from IONPs on the top surface of the sensor can be obtained from the following equations: $B_x = (\mu_0 Ma^3(a+t)d/((a+t)^2+d^2)^{5/2}, (y=0)$ for the vertical mode; and $B_x = (\mu_0 Ma^3/3((a+t)^2+d^2)^{3/2}, (x=0)$, $B_x = ((\mu_0 Ma^3/3((a+t)^2+d^2)^{3/2})((3d^2/((a+t)^2+d^2)^{5/3}-1)$,

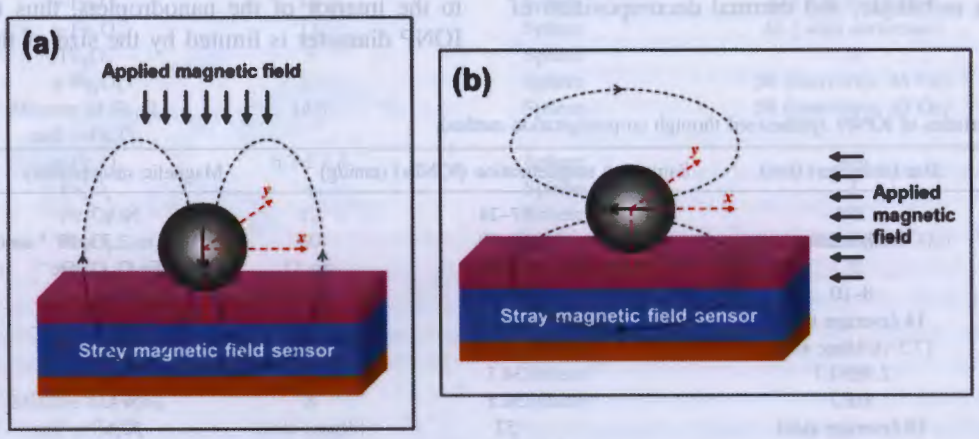

Fig. 3. Illustration of the stray magnetic field produced by magnetic iron oxide nanoparticle (IONPs) magnetized by the magnetic field in the (a) perpendicular and (b) parallel direction to the magnetic field sensor surface.

($y = 0$) for the in-plane mode.[26] From these equations, it can be found that the magnetization of IONPs and the distance separating the sensor from IONPs are two important parameters for the detection of magnetic stray field emanated by IONPs. Thus, in the design of these two detection schemes, thinner overlayer on the sensor surface, higher magnetization and smaller size of IONPs can induce stronger magnetic signal for the sensor detection.

The significant difference between these two modes is the zero-particle signal which is the signal output from the magnetic field sensor without the presence of IONPs. For the vertical mode, there is no signal output when no nanoparticle is presented. For the in-plane mode, there is a non-zero signal output from the sensor induced by the excitation magnetic field. Therefore, a reference is needed for the in-plane mode. The signal of IONPs can only be obtained by comparing the output signal of the sensor with its corresponding reference. For more information about the advantages and disadvantages of these two modes, one can refer to an excellent review about the giant magnetoresistance biosensors.[27]

3. SYNTHESIS AND SURFACE MODIFICATION OF IONPs

The significant advantage of IONPs in biomedical applications is that they are benign, nontoxic, and they are currently the only magnetic nanoparticle material approved by the U.S. Food and Drug Administration.[28] Besides, IONPs offer the advantage of multiple synthetic routes for their fabrication. There are numerous physical and chemical methods for the synthesis of IONPs which are well documented in literatures. The physical methods, for example ball milling and electrodeposition, can be adapted to mass production, but the size and shape of the nanoparticles are difficult to control.[29,30] Solution-based chemical methods have been investigated for the synthesis of IONPs with high quality. In this section, we briefly introduce three typical and representative chemical methods for the synthesis of IONPs, including co-precipitation method, micro-emulsion technique, and thermal decomposition of precursors.[31–33]

3.1. Co-Precipitation Method

The co-precipitation method is a simple way for the IONP synthesis. The synthesis of IONPs by alkaline precipitation of Fe^{3+} and Fe^{2+} ions was first introduced by Massart.[34] The formation of magnetite (Fe_3O_4) nanoparticles is through the chemical reaction: $Fe^{2+} + 2Fe^{3+} + 8OH^- \rightarrow Fe_3O_4 + 4H_2O$. Magnetite is not very stable and can be further oxidized into maghemite (γFe_2O_3) in the presence of oxygen: $Fe_3O_4 + 2H^+ \rightarrow \gamma Fe_2O_3 + Fe^{2+} + H_2O$. In Massart's synthesis, the IONPs were magnetite nanoparticles with a roughly spherical morphology of an 8 nm diameter. The Massart's synthesis technique has been adopted by other research groups, and the size of IONPs was varied from 2 nm to 17 nm by adjusting the acidity and ionic strength in the synthesis process.[35,36] This method does not require high temperature, and can be easily applied in large-scale production of IONPs. The products can be directly dispersed in water without further treatment. However, the synthesized IONPs are highly polydisperse and showed relatively poor crystallinity. Table I provides representative results including mean particle size and saturation magnetization value of the IONPs synthesized through the co-precipitation method. All of these samples are superparamagnetic with a roughly spherical morphology. However, very few literatures reported information about the magnetic susceptibility of IONPs samples.

3.2. Micro-Emulsion Method

Micro-emulsion method is also performed in aqueous solution similar to co-precipitation method, but the former offers better monodispersity control of IONPs products. The water-in-oil microemulsion consists of nanosized water droplets dispersed in an oil phase, offering a microenviroment for the formation of IONPs. The surfactant-covered water droplets limit the growth of IONPs, and the size of IONPs can be controlled by changing the ratio of water to surfactant, and the concentration of reactants.[44] However, the precipitated IONPs is confined to the interior of the nanodroplets, thus the range of an IONP diameter is limited by the size of the nanodroplets.

Table I. Characteristics of IONPs synthesized through co-precipitation method.

Type of IONPs	Size (diameter) (nm)	Saturation magnetization (IONPs) (emu/g)	Magnetic susceptibility	References
Fe_3O_4	2–4	17–24	N/A	[37]
Fe_3O_4	8.8 ± 2.7	65–70	1.1×10^{-3} to 2.3×10^{-3} emu (g of Fe_3O_4)$^{-1}$ Oe^{-1}	[38]
Fe_3O_4	8–10	77	N/A	[39]
Fe_3O_4	14 (average size)	68	N/A	[40]
Fe_3O_4	17.5 (average size)	65.4	N/A	[36]
γ-Fe_2O_3	2.9 ± 0.7	34.7	N/A	[41]
γ-Fe_2O_3	8 ± 2	50.5	N/A	[42]
γ-Fe_2O_3	10 (average size)	57	N/A	[39]
Fe_3O_4	10 (average size)	57	N/A	[43]
Fe_3O_4	11 (average size)	61.5	N/A	[25]

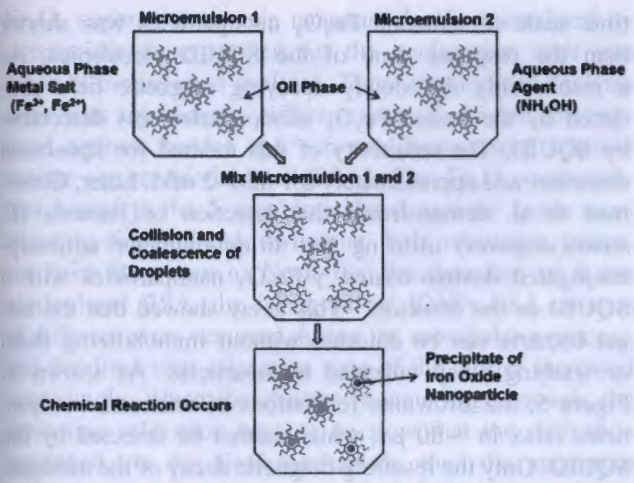

Fig. 4. Proposed mechanism for the formation of iron oxide nanoparticles (IONPs) through the microemulsion method.

The IONPs synthesized via microemulsion method often suffer from poor crystallinity, as compared to the ones via co-precipitation method. Figure 4 shows a typical method by mixing two microemulsions to produce IONPs.[44] There are two microemulisons prepared containing ferric and ferrous ion solution, and alkali solution, respectively. After mixing them together, interchange of the reactants occurs during the collisions of the water droplets. Then the nucleation and growth of iron oxide nanoparticles take place inside the droplets, which control the final size of the particles. Comparing with the other two synthesis methods (co-precipitation and thermal decomposition), the data about the IONPs obtained from micro-emulsion is relatively scarce, thus we do not list them in a table here. The IONPs syntheiszed through microemulsion might be a mixture of Fe_3O_4 and Fe_2O_3, with spherical morphology, usualy small in size (less than 15 nm) with narrow size distribution, displaying the saturation magnetization value between 10 emu/g to 50 emu/g.[45–48]

3.3. Thermal-Decomposition Method

Thermal decomposition of iron precusor in high-boiling-point solvents, with the presence of stabilizing surfactant, can produce high-quality monodisperse and monocrystalline iron oxide nanoparticles. The iron precusors utilized in thermal decomposition include iron acetylacetonate $Fe(acac)_3$, iron carboxylate FeO(OH), iron cupferronates $Fe(cup)_3$, hydrated ferric salts ($FeCl_3 \cdot 6H_2O$), and iron carbonyls $Fe(CO)_5$.[33,49–51] The commonly used stabilizing surfactants are oleylamine, oleic acid, and steric acid. Through the thermal decomposition of $Fe(acac)_3$, high-quality IONPs can be obtained with sizes ranging from 3 to 20 nm.[52] When iron carboxylate salts are used as precusors, the IONPs of 6 to 30 nm with narrow size distributions can be achieved.[33] IONPs with sizes ranging from 5 nm to 19 nm can be prepared by using $Fe(CO)_5$ as precusor.[53] The IONPs obtained through this method are usually hydrophobic, and require further phase transfer procedures to make them hydrophilic.[54,55] Table II provides some representative results of the IONPs synthesized through the thermal decomposition of various iron precursors. Through this method, the morphology of IONPs products can be controlled to be spherical or cubic. Their saturation magnetization values are between 3 emu/g to 84 emu/g.

4. RECENT ADVANCES ON THE MAGNETIC BIODETECTION WITH IONPs

As discussed previously, the main magnetic properties of IONPs employed in biodetection are magnetic relaxation,

Table II. Characteristics of IONPs synthesized through thermal decomposition method.

Iron precursor	Type of IONPs	Size (diameter) (nm)	Morphology of IONPs	Saturation magnetization (emu/g)	References
$Fe(CO)_5$	γ-Fe_2O_3	5	Sphere	23 (with surfactant)	[53]
$Fe(CO)_5$	γ-Fe_2O_3	19	Sphere	42 (with surfactant)	[53]
$Fe(CO)_5$	γ-Fe_2O_3	11	Sphere	46 (with surfactant)	[53]
$Fe(acac)_3$	Fe_3O_4	5	Sphere	27	[56]
$Fe(CO)_5$	γ-Fe_2O_3	12	Sphere	50 (coercivity: 45 Oe)	[56]
$Fe(CO)_5$	Mixture of Fe_3O_4 and γ-Fe_2O_3	14.5	Sphere	59 (coercivity: 45 Oe)	[56]
$Fe(Cup)_3$	γ-Fe_2O_3	6.7 ± 1.4	Sphere	N/A	[57]
$FeCl_3 \cdot 6H_2O$	Fe_3O_4	4	Sphere	3	[58]
$FeCl_3 \cdot 6H_2O$	Fe_3O_4	12	Sphere	59	[58]
$FeCl_3 \cdot 6H_2O$	Fe_3O_4	60	Cube	84 (coercivity: 85 Oe)	[58]
Iron oleate	Fe_3O_4	11 nm	Mixture of diamond, cubic and, triangular shaped particles	72	[59]
$Fe(acac)_3$	Fe_3O_4	6.9	Sphere	71	[59]
$Fe(acac)_3$	Fe_3O_4	5.7	Sphere	65	[59]
Iron oleate	Mixture of Fe_3O_4 and γ-Fe_2O_3	8 (side length)	Sphere	31	[60]
Iron oleate	Mixture of Fe_3O_4 and γ-Fe_2O_3	8 (side length)	Cube	40	[60]

magnetic permeability/susceptibility, and stray magnetic field. Accordingly, three general categories of magnetic biodetection schemes are developed based on these magnetic properties of IONPs.

4.1. Biodetection Based on Magnetic Relaxation of IONPs

In the detection mechanism based on magnetic relaxation of IONPs, IONPs are used as magnetic bio-markers for the specific detection of target biomolecules. The target biomolecules need to be bound with the IONPs, and this binding would suppress the Brownian relaxation of IONPs. Meanwhile, the unbound IONPs still undergo their original Brownian relaxation. Therefore, when the magnetic field applied to align their magnetic moments is switched off, the biomolecule-bound IONPs and unbound IONPs exhibit different relaxation behavior. With this phenomenon, the bound IONPs can be distinguished from the unbound IONPs due to their different magnetic relaxation times, and the unbound IONPs do not need to be washed away. As discussed previously, there are three main kinds of biodetection situations which can be realized in this detection scheme: the detection of small biomolecules when there is no crosslink, the detection of biomolecules through crosslinking process whereby IONPs forming clusters, and the detection of large immobile biomoleculesin suspension or bioanalytes attached onto a solid substrate. In this section, we summarize the recent research progress in the biodetection based on magnetic relaxation of IONPs, in which the relaxation signal is mainly measured through magnetorelaxometry using superconducting quantum interference devices (SQUID), fluxgates, or magnetoresistive (MR) sensor.

SQUIDs have been used to detect the magnetic relaxation signal of magnetic nanoparticles, as they have the highest sensitivity among solid-state magnetic field sensors. A homogenous magnetic immunoassay based on the measurement of magnetic bio-markers bound onto a substrate using a SQUID has been developed by Chemal et al.[15] The IONPs used in their study were Fe_3O_4 nanoparticles with size of around 20 nm. For an ideal single-domain 20-nm Fe_3O_4 nanoparticle, the Brownian relaxation time (τ_B) and Neel relaxation time (τ_N) are $\tau_B \sim 1\ \mu s$ and $\tau_N \sim 1$ s respectively, indicating its relaxation behavior is dominated by Brownian relaxation. A plastic film bound with target liposomes served as substrate. The liposomes carried the human CCR5 receptor, which were altered to carry the FLAG epitope. After the addition of a suspension of Fe_3O_4 nanoparticles carrying antibodies which direct against the liposomes, the nanoparticles bound to the target liposomes became immobilized and underwent Neel relaxation. The unbound nanoparticles relaxed by Brownian rotation after the magnetic field was turned off. The measurement speed of the SQUID was between 1 ms and 1 s. The Brownian-relaxation time scale of unbound Fe_3O_4 nanoparticles was shorter than the response time of the SQUID electronics. As a result, only the slowly decaying magnetic field produced by the bound Fe_3O_4 nanoparticles was detectable by SQUID. The sensitivity of this method for liposomes detection was approximately 0.1 mM–2 mM. Later, Grossman et al. demonstrated the detection of bacteria (*L. monocytogenes*) utilizing the 50-nm-diameter antibody-conjugated dextran-coated γ-Fe_2O_3 nanoparticles with a SQUID as the detector.[61] This assay showed that the target bacteria can be detected without immobilizing them or washing away unbound nanoparticles. As shown in Figure 5, the Brownian relaxations of unbound nanoparticles relax in $\sim 50\ \mu s$, which cannot be detected by the SQUID. Only the resulting magnetic decay of the nanoparticles bound to the relatively large bacteria rotated slowly and underwent Neel relaxation can be detected by SQUID. The sensitivity in this measurement was 1.1×10^5 bacterial in a 20 μl sample volume.

Comparing with a SQUID, a fluxgate is a simple instrument which does not require any cryogenic cooling or complicated magnetic shielding. Hence it has the potential to be applied in compact magnetic biodetection systems. A differential fluxgate system operating at room temperature to detect magnetic relaxation signal of IONPs was introduced by Heim et al. in recent years.[62] Different from a SQUID which only detects magnetic flux changes, a fluxgate measures the absolute value of the magnetic field in the sensitive axis.[63] In Ludwig's study, 100 nm

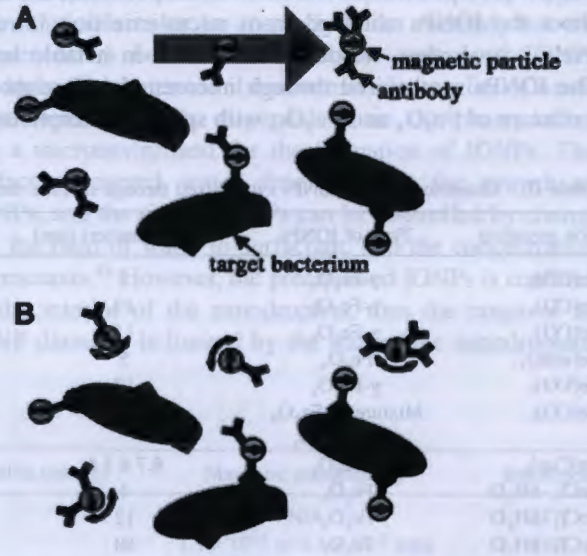

Fig. 5. Principle of a SQUID-based homogeneous detector of bacteria. (A) Magnetic moments of IONPs are oriented by applied magnetic field. (B) Brownian motion randomizes the magnetic moments of unbound IONPs after the removal of magnetic field. The bacterial-bound IONPs undergo Neel relaxation, and the unbound IONPs undergo Brownian relaxation. The SQUID detects the slower Neel relaxation for the bacterial-bound IONPs. Reprinted with permission from [61], H. Grossman, et al., *Proc. Natl. Acad. Sci.* 101, 129 **(2004)**. © 2013, National Academy of Sciences, U.S.A.

Fe_3O_4 superparamagnetic nanoparticles functionalized by streptavidin were applied for the conjugation with two types of biotinylated analytes. These biotinylated analytes were with significantly different sizes of ~5 μm (biotinylated agarose beads) and ~6 nm (biotinylated albumin bovine serum, biotinylated BSA). The Fe_3O_4 nanoparticles bound to the 5 μm biotinylated agarose beads were instantly immobilized, switching their relaxation behavior from Brownian to Neel. For the detection of 6 nm biotinylated BSA, the formation of IONPs-BSA clusters of different sizes occurred during the crosslinking process, and the Brownian relaxation time of the cluster increased accordingly. When the clusters became large enough, the Brownian relaxation became so slow that the relaxation happened via the Neel mechanism, thus the maximum relaxation time constant was reached. In Heim's work, for the detection of agarose beads, the use of 10 ng IONPs led to a lower detection limit of 1.25 μl and an upper detection limit of 27.5 μl. For the BSA analytes, the detected concentration range was about 14–71.3 μmol/l.

MR sensors are the main competitors to fluxgate sensors and SQUIDs since MR sensors are simpler and cheaper.[64,65] In addition, commercially available MR sensors are even smaller than fluxgates and consume less energy.[64] Recently, Bhuiya et al. successfully utilized MR sensors as a magnetorelaxometry detector for detecting magnetic biotargets.[66] The Fe_3O_4 nanoparticles with hydrodynamic size of 110 nm were used as magnetic biolabels. For biodetection purpose, polymer beads with diameter of 3.3 μm were used to fix the biological targets. The Fe_3O_4 nanoparticles conjugated with biological targets bound onto the beads whereas the others remained free. The Brownian relaxation of the Fe_3O_4 nanoparticles bound onto the beads was dominated by the volume of the polymer beads, and the relaxation time became $\tau_B = 10$ s. The unbound Fe_3O_4 nanoparticles showed rapid relaxation with relaxation time $\tau_F = 0.5$ ms. The magnetic relaxation signal M_B from the bound Fe_3O_4 nanoparticles could be measured by MR sensor at time T ($\tau_F \ll T \ll \tau_B$) after the excitation field was removed, while the signal M_F from the free Fe_3O_4 markers became zero. As shown in Figure 6, a disk-shaped sample plate rotated by an ultrasonic motor was used to ensure the signal M_B from the bound Fe_3O_4 nanoparticles could be measured by the MR sensor (HMC1001, Honeywell, USA) at time $T = 1.5$ s. Then, the amount of the biological targets can be quantitatively determined from the signal M_B of bound Fe_3O_4 markers. In this study, the minimum detectable number of Fe_3O_4 markers is 1.4×10^7. For the detection of biotins, the sensitivity of this method was 3.8×10^{-16} mol/ml. Later, Bhuiya et al. used the similar detection scheme to perform the detection of biotin by using three detectors: a SQUID, an MR sensor, and a fluxgate.[67] The sensitivities of SQUID, MR sensor, and fluxgate were 5.6×10^{-18} mol/l, 2.8×10^{-16} mol/l and 2.8×10^{-16} mol/l, respectively, in terms of the molecular-number concentration of biotins.

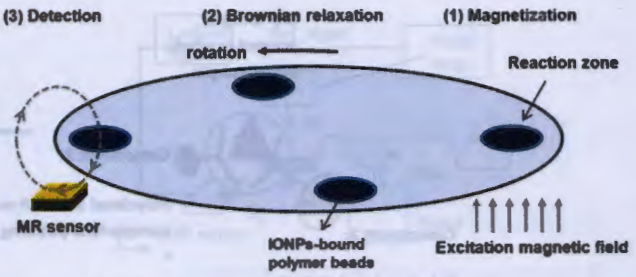

Fig. 6. Detection system based on magnetic relaxation measurement by using magnetoresistive (MR) sensor. Biotargets were prefixed on polymer beads, and iron oxide nanoparticles (IONPs) could be conjugated with biological targets, forming the final complex IONPs-bound polymer beads.[66]

In Bhuiya's study, they noticed that the magnetic signal strength measured by the fluxgate was significantly smaller than that measured by the MR sensor. They proposed that the main reason is the rapid decay of signal with distance. The distance between the sample and the MR sensor (or the SQUID) can be set as around 1.5 mm, while the distance must be longer than 5 mm for the fluxgate because of its thick enclosure.

4.2. Biodetection Based on Magnetic Permeability/Susceptibility of IONPs

The relative magnetic permeability (μ_r) of a material provides a measure of the material's ability to respond to an externally applied magnetic field, and it does not change with the conjugation of a biotarget. Inductance-based magnetic permeability detector is the main instrument used for the measurement of magnetic biolabels based on their permeability. A biosensor based on measurement of magnetic permeability was developed by Kriz et al. in 1996.[18] When a magnetic nanoparticle is placed inside a coil, the inductance of the coil changes due to the permeability of the particle. However, the permeability of magnetic nanoparticle does not change whether it is bound with biotarget or not. Thus, a separation of biotarget-bound IONPs and unbound IONPs was needed before the final signal measurement. Recently, Ibraimi et al. realized the detection of C-reactive protein (CRP) through a magnetic permeability based immunoassay. utilizing the 70 nm dextran-coated superparamagnetic IONPs, silica microparticles (15 to 40 μm), and inductance-based magnetic permeability detector.[68] CRP is identified as a useful acute phase marker for diagnosis and monitoring of inflammatory disease. As shown in Figure 7, the polyclonal anti-CRP coated IONPs and polyclonal anti-CRP coated silica microparticles formed a sandwich complex through the conjugation with CRP antigens. The complex subsided to the bottom of the vial, and its signal can be measured by the magnetic permeability detector. The output signal of the coil exhibits a linear relation with the relative magnetic permeability μ_r of the magnetic sediments. In this

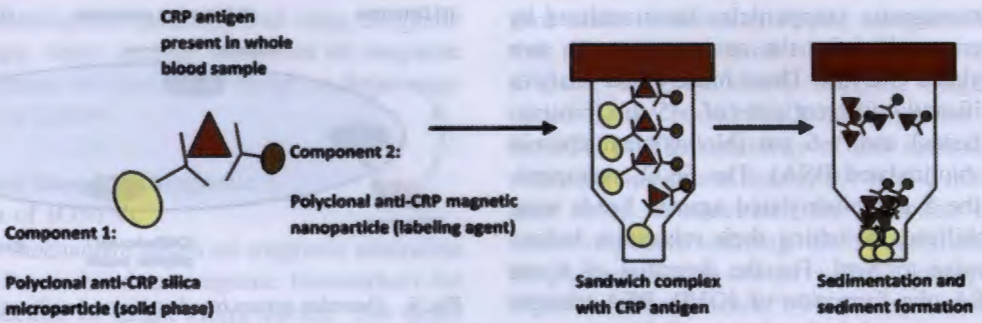

Fig. 7. An illustration of the principle of the one-step magnetic permeability based two-site immunoassay technology. The CRP antigen present in the whole blood sample forms a sandwich complex with the polyclonal anti-CRP magnetic nanoparticle (labeling agent) and the polyclonal anti-CRP silica microparticle (solid phase) present in the reagent vial. The sandwich complex starts to sediment to the bottom of the reagent vial due to the large density. After completed sediment formation the reaction signal of the sandwich complex sediment in the vial can be measured by placing the vial into the coil of the magnetic permeability detector. Reprinted with permission from [68], F. Ibraimi, et al., *J. Magn. Magn. Mater.* 321, 1632 **(2009)**. © 2013, Elsevier.

REVIEW

study, the detection limit for the lowest CRP concentration was determined to be 1.7 mg/l.

For magnetic fluids, the complex susceptibility is frequency dependent and it is related to the hydrodynamic sizes of the particles as discussed previously. Since the Brownian relaxation behavior of IONPs in solution is also dependent on their hydrodynamic sizes, the three kinds of detecting mechanisms based on magnetic relaxation are also applicable in the biodetection scheme with magnetic complex susceptibility. The main detectors used in the detection based on the complex susceptibility of IONPs are AC susceptometers, photodetectors (magneto-optical measurement), SQUIDs, and MR sensors. There are advantages and limitations for each of these detectors.

Different from the biodetection based on the permeability of IONPs, the detection based on complex susceptibility does not need the separation of unbound IONPs from the biotarget-bound IONPs. In the magnetic detection, only the frequency ω at which $\chi''(\omega)$ reaches its maximum is measured experimentally. Generally speaking, for the IONPs dominated by Brownian relaxation, the frequency ω of the maximum $\chi''(\omega)$ decreases as the hydrodynamic size of IONPs increases after the binding of biomolecules. The use of AC susceptometry for the detection of biomolecules using tagged magnetic nanoparticles was first proposed theoretically by Connolly and St Pierre.[69] A platform for multiplex detection based on Brownian relaxation of IONPs using a compact AC susceptometer was proposed by Park et al. in 2011.[70] The proposed compact AC magnetic susceptometer consists of a high impedance AC current source, precise millimeter-sized differential sensing coils, and a lock-in amplifier. Streptavidin coated Fe_3O_4 nanoparticles (25 nm) were used in Park's study to detect the biotinylated horseradish peroxidase (HRP). Corresponding to the different hydrodynamic sizes of IONPs, the imaginary component of the AC susceptibility of IONPs has their own distinct frequency peak. Thus, an AC susceptometer enables the detection of multiple frequency peaks for a mixture of differently sized IONPs simultaneously. As shown in Figure 8, the frequency peak of the AC magnetic imaginary susceptibility of IONPs exhibits an expected shift upon avidin-biotin conjugation which induced the cluster formations with various sizes. The sensitivity of the compact AC susceptometer is 1 mg/ml concentration under a magnetic field as low as 10 μT.

Magneto-optical measurement is a relatively new and simple technology as compared to the traditional AC susceptometry, and has recently been proposed to measure Brownian relaxation of magnetic nanoparticles to acquire AC magnetic susceptibility as a function of frequency.[71] It can operate at room temperature and does not need expensive cryogenics. A one-step homogeneous magnetic immunoassay for prostate specific antigen (PSA) in human blood plasma was demonstrated by Ranzoni et al. using magneto-optical measurement.[72]

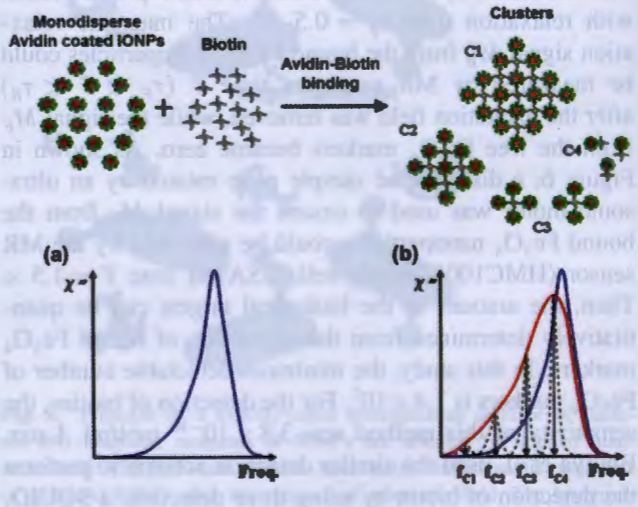

Fig. 8. Schematic representation of imaginary part of AC magnetic susceptibility of (a) monodisperse avidin coated IONPs and (b) clusters of IONPs upon avidin-biotin interaction. Reprinted with permission from [70], K. Park, et al., *Nanot.* 22, 085501 **(2011)**. © 2011, IOP Publishing.

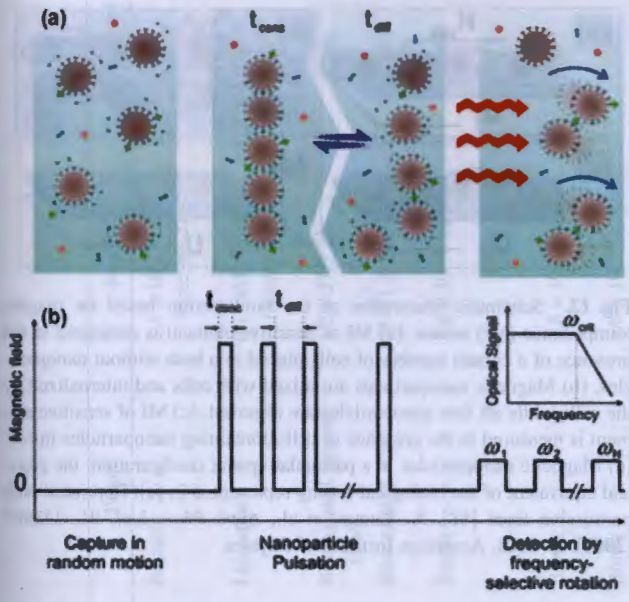

Fig. 9. Principle of the one-step homogeneous assay technology based on magnetic nanoparticles and magneto-optical measurement. The assay proceeds in three phases, controlled by the applied magnetic field (see panel (a)): capture, pulsation, and detection. During the detection phase, the clusters are magnetically rotated and thereby generate a modulation of optical scattering. The result is a curve of optical scattering signal as a function of frequency (see panel (b)). Reprinted with permission from [72], A. Ranzoni, et al., *ACS Nano* 6, 3134 **(2012)**. © 2013, American Chemical Society.

Carboxyl-coated nanoparticles (500 nm Masterbeads) were used here to conjugate with PSA antibodies. As shown in Figure 9(a), the assay proceeds in three phases. Firstly, the PSA molecules were captured by antibody-functionalized nanoparticles. Secondly, a pulsating magnetic field concentrated the nanoparticle in chains, and the nanoparticles diffused by Brownian motion (during t_{diff}), which facilitated biomarker-induced inter-nanoparticle binding. During this stage, the nanoparticle concentrating and nanoparticle diffusing happen alternately. Finally, the clusters of nanoparticles caused by inter-particle binding were sensitively detected by optical scattering at the applied magnetic field rotation frequencies.[73] The optical scattering signal was measured by a photodetector as a function of the field rotation frequency. The cluster number is reflected by the plateau signal, and the value of critical frequency (ω_{crit}) represents the size of clusters (Fig. 9(b)). The detection limit of this method for the detection of PSA in undiluted human blood plasma was 400–500 femtomol/l.

Comparing to traditional AC susceptometry and magneto-optical measurement, a MR sensor is simpler and smaller to be used for the magnetic field detection with high sensitivity, and it can operate at room temperature.[27] The detection of biotin-conjugated polystyrene (6.7 μm) with avidin-coated Fe_3O_4 nanoparticles (20 to 25 nm) based on the susceptibility measurement has been performed by Enpuku et al. using MR sensors.[74] As shown in Figure 10, the sample was placed on a disk-shaped

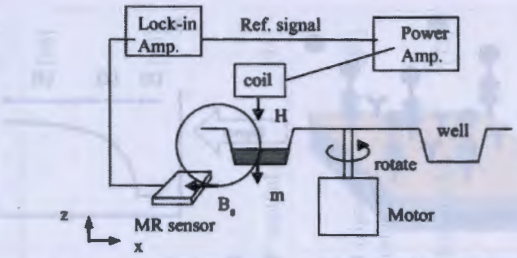

Fig. 10. Experimental circuit for the measurement of AC susceptibility of magnetic markers in solution using MR sensor. The sample was placed on a disk-shaped sample plate, rotated by an ultrasonic motor, and magnetized by an AC excitation field provided by the excitation coil. The signal field generated by the magnetic moment of nanoparticles was detected by a MR sensor, which was connected to the lock-in amplifier in order to obtain both the real and imaginary parts of the signal. Reprinted with permission from [74], K. Enpuku, et al., *J. Appl. Phys.* 108, 034701 **(2010)**. © 2013, American Institute of Physics.

sample plate, rotated by an ultrasonic motor, and magnetized by an AC excitation magnetic field provided by an excitation coil. The signal field generated by the magnetic moment of IONPs was detected by a MR sensor, which was connected to the lock-in amplifier in order to obtain both the real and imaginary parts of the signal. The sensitivity of this detection system using MR sensor was 1.3×10^{-16} mol/ml in terms of the molecular-number concentration of the markers.

4.3. Biodetection Based on Stray Magnetic Field of IONPs

Stray magnetic field is generated by the magnetization of IONPs, and detection of such field usually needs to be performed upon a solid-state sensor. In the magnetic biodetection, the biomolecule-bound IONPs are immobilized on the sensor surface through the bio-conjugation in either complementary bioassay way or sandwich immunoassay way as discussed previously. The unbound IONPs need to be washed away, and only the magnetic stray field from the bound magnetic nanoparticles is detected by the magnetic field sensor. The detected signal reflects the presence of the target bioanalytes. The most commonly used detectors in recent years include giant magnetoresistive (GMR) sensors, magnetic tunnel junction (MTJ) sensors, and giant magnetoimpedance (GMI) sensors. All these sensors possess the obvious advantages of low cost and high sensitivity comparing with many other magnetometers, such as Hall effect magnetometers and SQUID magnetometers.[75,76]

MR effect is the change of electrical resistance in material in response to an external magnetic field. The maximum signal that can be obtained from the MR sensor is indicated by MR ratio. The MR ratio is traditionally defined in terms of maximum resistance and minimum resistance of the sensor, by $MR\% = ((R_{max} - R_{min})/R_{min}) \times 100\%$. More detailed explanations about MR ratio can be found in the Ref. [77]. A GMR sensor is very sensitive to

REVIEW

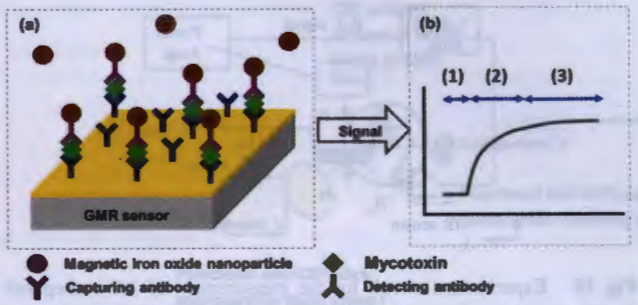

Fig. 11. Schematic illustration of (a) the magnetic IONP-based immunoassay for mycotoxins. IONPs are bound onto the GMR sensor surface through the sandwich immunoassay of mycotoxins, and the detection of stay magnetic field signal in real time. (b) Typical signal curve for the IONP binding: (1) signal baseline before the addition of IONPs; (2) binding kinetics upon the addition of IONPs; and (3) signal saturation achieved when the IONPs saturated the available binding sites on the GMR sensor.[80]

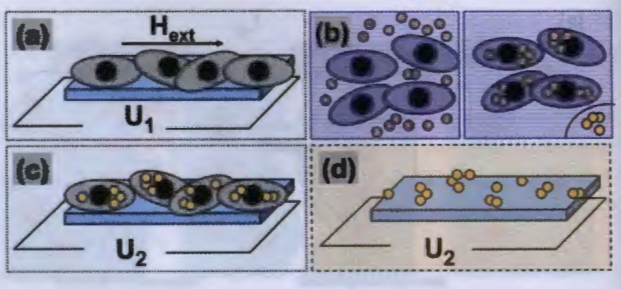

Fig. 13. Schematic illustration of the biodetection based on magnetoimpedance (MI) sensor. (a) MI of sensitive element is measured in the presence of a certain number of cells placed in a bath without nanoparticles. (b) Magnetic nanoparticles are mixed with cells and internalized by the cells while all free nanoparticles are removed. (c) MI of sensitive element is measured in the presence of cells containing nanoparticles inside. (d) Magnetic nanoparticles in a particular spatial configuration, the physical equivalent of the biological testing represented in (c). Reprinted with permission from [88], A. Kumar, et al., *Appl. Phys. Lett.* 91, 143902 (**2007**). © 2013, American Institute of Physics.

the change of magnetic field, and is compatible with the standard CMOS fabrication technology. Thus, it has a great promise for low-cost and high-sensitive lab-on-chip biodetection application. Since the first report of using GMR sensors to detect the stray magnetic field of magnetic particles tagged to biotargets by Baselt et al. in 1998,[78] it has become a much sought-after research topic in recent years, particularly with the advances in nanofabrication techniques. Recently, the multiplexing detection of cancer markers or mycotoxins has been realized through the integration of the classic sandwich-based immunoassay with IONPs and GMR sensors.[79,80] Mak et al. carried out the detection of mycotoxins in 2010.[80] They used a cluster of Fe_2O_3 superparamagnetic nanoparticles within a dextran matrix, with the overall diameter of around 50 nm. Figure 11(a) shows the schematic illustration of the IONP-based immunoassay for mycotoxins upon the GMR sensor surface, and Figure 11(b) displays the detection of IONP stray magnetic field signal in real time. Before the addition of IONPs, there is a signal baseline in the GMR sensor. The signal increases as the IONPs bind onto the sensor surface through the sandwich immunoassay of mycotoxins. When the IONPs saturate the available binding sites on the GMR sensor, the signal reaches the maximum which represents the amount of the mycotoxins detected in the assay. The simultaneous detection of three mycotoxins (aflatoxin-B1, zearalenone and HT-2) was demonstrated with a detection limit of 50 pg/ml. Apart from mycotoxins, multiplexing protein detection of cancer markers was also demonstrated by Oeterfeld et al. at subpicomolar concentration levels by utilizing the IONPs with size of around 50 nm.[79] Furthermore, Gaster et al. demonstrated the quantification of protein interactions and solution transport by using a high-density GMR sensor arrays.[81] The IONPs used in their study were dextran-coated Fe_2O_3 clusters with entire size of 46 nm $\pm$13 nm. The kinetics of antibody-antigen binding can be quantified at sensitivities as low as 20 zeptomoles of solute.

Comparing with GMR sensors, MTJ sensors offer even higher MR ratio and therefore, MTJ sensors are expected to have higher sensitivity at low magnetic field. However,

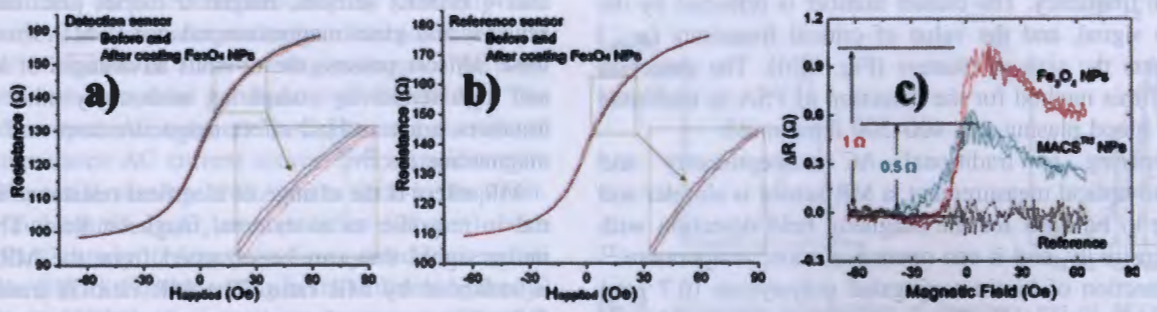

Fig. 12. The MR transfer curves measured before and after the binding of Fe_3O_4 nanoparticles, (a) from an MTJ array treated with DNA and (b) from a nearby array without DNA treatment, meant as a reference. (c) Measured resistance differences for the detection sensors bound with Fe_3O_4 and MACS™ nanoparticles through DNA hybridization, respectively, and for the reference sensor. Reprinted with permission from [82], W. Shen, et al., *J. Appl. Phys.* 103, 07A306 (**2008**). © 2013, American Institute of Physics.

Table III. Biodetection configuration and sensitivity based on the magnetism of IONPs.

Magnetism of IONP	(IONPs structure)	IONPs (preparation)	IONPs (size)	Signal detector	Target	Sensitivity	References
Magnetic relaxation signal	Antibody-conjugated dextran-coated γ-Fe_2O_3	From Miltenyi Biotec, Auburn, CA	10 nm (core) 50 nm (hydrodynamic)	SQUID	Bacteria	1.1×10^5 bacterial/20 μl	[61]
	Fe_3O_4	From Quantum Magnetics, Madison, CT	35 ± 5 nm (core) 56 nm (hydrodynamic)	SQUID	Liposome	0.1 mM–2 mM liposome	[15]
	Streptavidin functionalized Fe_3O_4	From Chemicell GmbH, Germany	100 nm (hydrodynamic)	Differential fluxgate system	Biotinylated agarose beads	1.25–27.5 μL	[62]
	Streptavidin functionalized Fe_3O_4	From Chemicell GmbH, Germany	100 nm (hydrodynamic)	Differential fluxgate system	Biotinylated BSA	14–71.3 10^{-6} mol/L	[62]
	Fe_3O_4	From Magcellect particles, R&D Systems, USA	20~25 nm (core) 110 nm (hydrodynamic)	MR sensor (HMC1001, Honeywell, USA)	Biotin	3.8×10^{-16} mol/mL	[66]
	Fe_3O_4	From R&D System, Magcellect	112 nm (hydrodynamic)	Fluxgate (Bartington)	Biotin	2.8×10^{-16} mol/mL	[67]
	Fe_3O_4	From R&D System, Magcellect	112 nm (hydrodynamic)	Home-made high-Tc SQUID	Biotin	5.6×10^{-16} mol/mL	[67]
	Fe_3O_4	From R&D System, Magcellect	112 nm (hydrodynamic)	MR sensor (Honeywell)	Biotin	2.8×10^{-16} mol/mL	[67]
Magnetic permeability	Dextran coated IONPs	Co-precipitation	70 nm (hydrodynamic)	Inductance-based magnetic permeability detector	Canine C-reactive protein (CRP)	1.7 mg/L	[68]
Magnetic susceptibility	Streptavidin coated Fe_3O_4	From Ocean Nanotech, USA (Thermal decomposition)	25 nm (core)	A compact AC susceptometer	Biotinylated horseradish peroxidase (HRP)	1 mol/mL	[70]
	Avidin-coated Fe_3O_4	From MagCellect particles, R&D Systems, U.S.A.	20–25 nm (core) 110 nm (hydrodynamic)	MR sensor	Biotin-conjugated polystyrene	1.3×10^{-16} mol/mL	[74]
	Amino group functionalized dextran-coated γ-Fe_2O_3	From Micromod Partikeltechnologie, Germany	130 nm (hydrodynamic)	SQUID	DNA	3~10 pM (signal amplification)	[89]
	Carboxyl-coated IONPs	From AdemTech	500 nm (hydrodynamic)	Photodetector (magneto-optical measurement)	Prostate specific antigen (PSA)	400–500 femtomol/L	[72]

Table III. Continued.

Magnetism of IONP	(IONPs structure)	IONPs (preparation)	IONPs (size)	Signal detector	Target	Sensitivity	References
Stay magnetic field	Streptavidin coated Fe_3O_4	Home-made in laboratory	16 nm	MTJ sensor	DNA	100 nM	[83]
	Carboxyl-group functionalized Fe_3O_4	From Ocean Nanotech (Thermal decomposition)	20 nm	MTJ sensor	Alpha-fetoprotein (AFP)	0.002 mg/mL	[84]
	Fe_3O_4	Co-precipitation	30 nm	GMI sensor	Fe_3O_4 nanoparticles embedded in human embryonic kidney (HEK 293) cells	$\sim 10^5$ particles/cell	[88]
	Clusters of Fe_2O_3 nanoparticles within a dextran matrix and prefunctionalized with streptavidin	From Miltenyi Biotec Inc.	10 nm (core) 50 nm	GMR sensor	Aflatoxins B1, zearalenone and HT-2	50 pg/mL	[80]
	Clusters of Fe_2O_3 nanoparticles embedded in a dextran polymer and prefunctionalized with streptavidin	From Miltenyi Biotec Inc.	10 nm (core) 50 nm	GMR sensor	Multiple tumor markers (protein)	10 ng/mL	[90]
	Streptavidin coated magnetic IONPs	From, Miltenyi Biotec Inc., Auburn, CA	50 nm	GMR sensor	Tumor markers (protein)	1 pg/mL	[91]
	Clusters of Fe_2O_3 nanoparticles within a dextran matrix and prefunctionalized with streptavidin	From Miltenyi Biotec Inc., Auburn, CA	10 nm (core) 50 nm	GMR sensor	Human Papillomavirus (HPV) DNA	10 pM	[92]
	Commercial MACS™ IONPs	From Miltenyi Biotec	50 nm	MTJ sensor	DNA	2.5 μM	[82]

they are still in a relatively infant phase of development. In 2008, Shen et al. reported the design of the first magnetic biosensors based on MTJ sensor arrays with MgO barrier.[82] They demonstrated the detection of 2.5 μM target DNA labeled with 16 nm Fe_3O_4 nanoparticles and 50 nm commercial MACS™ IONPs using the MgO-based MTJ sensor arrays. Figure 12 shows the MR transfer curve of the MTJ sensor measured before and after the binding of the IONPs through DNA hybridization. The measured resistance differences represent the amounts of IONP binding onto the sensor surface, thus indicating the presence of the target DNA elements (Fig. 12(c)). Based on the same principle, the quantitative real-time detection of DNA was realized by using 64-element MTJ bridge array and 16 nm Fe_3O_4 nanoparticles.[83] The detection limit of complementary target DNA through this system was further improved to be better than 100 nM. Recently, Lei et al. explored the detection of a cancer marker (alpha-fetoprotein antigen) with 20 nm carboxyl-group functionalized Fe_3O_4 nanoparticles and MgO-based MTJ sensors by a sandwich-assay configuration.[84] It was found that the increase of resistance variation of the same MTJ sensor is in proportion to the logarithm of the detecting AFP antigen concentration. The lowest detectable concentration of AFP antigen is 0.002 mg/ml.

GMI effect is the significant change of the impedance value of a magnetic conductor (wire, ribbon, thin layers) passed by a high frequency current in response to an applied DC magnetic field is applied.[85] Similar to MR sensors, GMI sensors also offer the features of low cost and high sensitivity. It was reported that GMI sensors can have higher sensitivity than traditional GMR sensors, although the development of GMI sensors is still in an early stage.[86,87] In 2007, the magnetoimpedance (MI) sensor was successfully used to conduct the detection of Fe_3O_4 nanoparticles (30 nm) uptake by human embryonic kidney (HEK 293) cells. [88] An amorphous ribbon exhibiting large MI served as the sensor in this detection. An excitation magnetic field was applied to magnetize the Fe_3O_4 superparamagnetic nanoparticles for emanating the magnetic stray field signal. As shown in Figure 13, the effective magnetic field experienced by the sensor depends on whether the cells contain the IONPs. The magnetic stray field emanated from the IONPs alters the applied constant excitation field, and the alternating field can be detected through the impedance change of the sensor. The IONPs were embedded inside HEK 293 cells with a concentration of $\sim 10^5$ particles/cell. The presence of the IONPs after intracellular uptake was successfully detected by this MI biosensor. Recently, Chen et al. also realized a targeted detection of gastric cancer cells by combining the GMI-based biodetection system and chitosan coated Fe_3O_4 nanoparticles (20 nm).[86] The IONP-targeted cells can be detected and identified by the difference in GMI ratio. More detailed explanation about the GMI ratio can be found in Ref. [86].

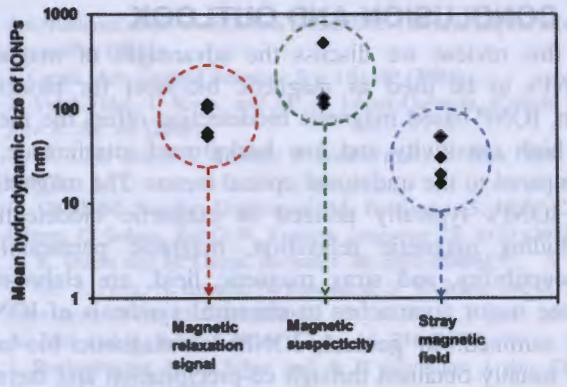

Fig. 14. Distribution of the mean hydrodynamic size of IONPs for the three kinds of magnetic biodetection methods based on different magnetism of IONPs.

Table III displays a review of magnetic biodetection configurations and the IONPs used in recent literature. Both Fe_3O_4 and γ-Fe_2O_3 were used as magnetic labels in these three kinds of magnetic biodetection, and they were mainly prepared through the co-precipitation method and thermal decomposition method. Many of the IONPs tags are nowadays commercially available. The distribution of IONP hydrodynamic size for the magnetic biodetections based on different magnetism of IONPs is shown in Figure 14. It can be found that the particle size plays an important role here. The hydrodynamic sizes of the IONPs used in biodetection based on magnetic relaxation and susceptibility are generally larger than the ones used in the biodetection based on stray magnetic field. The particle size used for magnetic relaxation signal ranges from 50 to 112 nm, and for magnetic susceptibility, it ranges from 110 nm to 500 nm. However, for the magnetic stray field, the particle size ranges only between 16 nm to 50 nm. Different sizes of IONPs are used in these three kinds of magnetic biodetection schemes mainly due to the different detection mechanism they utilize. In the detection based on magnetic relaxation or magnetic susceptibility, the unbound particles and bound particles are distinguished by their different Brownian relaxation time or different frequency ω of maximum imaginary component of complex magnetic susceptibility. Both require the particles to be suitably sized on which Brownian relaxation is faster than Neel relaxation. As discussed previously, there usually exists a critical size above which the Brownian relaxation mechanism becomes dominant ($\tau_N \gg \tau_B$), and the critical size of an ideal single-domain spherical IONP at room temperature is about 20 nm.[15] Thus, the IONPs with size of above 50 nm are commonly used in literature in order to ensure they are larger than the typical critical size. In the detection based on magnetic stray field, there is no such size restriction, and the superparamagnetic IONPs with comparable size as the biotargets are preferable for the biodetection with high-sensitivity. Thus the IONP size used for magnetic stray field in literature is mainly below 50 nm.

REVIEW

5. CONCLUSION AND OUTLOOK

In this review, we discuss the advantages of magnetic IONPs to be used as magnetic bio-label for biodetection. IONP-based magnetic biodetection offers the merits of high sensitivity and low background interference, as compared to the traditional optical means. The magnetism of IONPs typically utilized in magnetic biodetection, including magnetic relaxation, magnetic permeability/susceptibility, and stray magnetic field, are elaborated. Three major approaches to chemical synthesis of IONPs are outlined. In general, IONPs as magnetic bio-label are usually obtained through co-precipitation and thermal decomposition. The major advantage of co-precipitation is that this method can be easily applied in large-scale production of IONPs, and the IONP products can be directly dispersed in water. On the other hand, IONPs obtained through thermal decomposition provide significant advantages such as high-level uniformity and monocrystallinity, as compared to nanoparticles synthesized through co-precipitation and microemulsion. Furthermore, the recent progresses in the three different categories (magnetic relaxation, magnetic permeability/susceptibility, and stray magnetic field) of IONP-based magnetic biodetection schemes are discussed. Finally, various kinds of magnetic IONPs used as biolabels and their corresponding magnetic detectors are overviewed. Many of the IONPs tags and magnetic detectors are already commercially available and can be easily acquired from different companies. Their sources have been summarized for reference.

The main trend for the magnetic biodetection configuration is to achieve multiplexing sensing and miniaturization. Since the biomolecule-bound IONPs and unbound IONPs exhibit different relaxation time and different frequency ω of maximum imaginary component of complex magnetic susceptibility, the biodetection mechanisms based on magnetic relaxation and magnetic susceptibility are especially suitable for multiplexing sensing. In these two biodetection mechanisms, no separation of the bound and unbound IONPs is needed, and the multiple biotargets can be detected simulatously by one detector. The traditional detectors including SQUIDs and AC susceptometers need complicated equipment and thus they are not favourable for miniaturization, while the fluxgates and MR sensors with much smaller size have been emerged as better options. However, there is a criteria needs to be fulfilled which is the magnetic tags must be suitably-sized IONPs on which Brownian relaxation is much faster than Neel relaxation. This is the reason that most of the IONPs used in literature have size larger than 50 nm. It is known that the size of IONP tags should be comparable with biological targets including proteins with sizes of few nanometers. The requirement on the particle size due to relaxation might limit these two detection configurations in the high-precision biodetection of very tiny biotargets, for example, with the size less than 50 nm.

On the other hand, there is no such size limitation on IONPs in the biodetection based on magnetic permeability and stray magnetic field. Superparamagnetic IONPs with high saturation magnetization are the best candidates in these two kinds of detection. However, the permeability and stray magnetic field of IONPs remain the same when they are bound or unbound with biomolecules. The separation of bound and unbound IONPs is needed before the signal sensing. The detection for magnetic permeability of IONPs is mainly carried out by using inductance-based magnetic permeability detector. The IONPs need to be inserted into the coil which is difficult for multiplexing sensing because of the wash-away space limitation and particle separation procedures. While the detection of stray magnetic field occurs mainly upon the sensor surface, the wash-away procedure can be easily handled by using microchannel. The multiplexing sensing of different bioanalytes can be achieved by pre-immobilizing different capturing molecules on different working areas on a sensor array. Since the GMR, MTJ, and GMI sensors are all of low cost and with high sensitivity, they are promising candidates for the detection of small biomolecules with high precision based on magnetic stray field of IONP tags. Therefore, by utilizing appropriate combination of IONPs and magnetic sensors as biolabels and signal detectors, it can be foreseen that the IONP-based magnetic biodetection will manifest its great potential as a multiplexing and miniaturizable testing platform for medical application.

Acknowledgments: We acknowledge the financial support by the Seed Funding Program for Basic Research and the Small Project Funding from the University of Hong Kong, the RGC-GRF grant (HKU 704911P), and University Grants Committee of Hong Kong (Contract No. AoE/P-04/08).

References and Notes

1. N. Sanvicens, C. Pastells, N. Pascual, and M. Marco, *Trends Anal. Chem.* 28, 1243 (**2009**).
2. X. Sun, D. Ho, L.-M. Lacroix, J. Q. Xiao, and S. Sun, *IEEE Trans Nanobioscience* 11, 46 (**2012**).
3. W. Wang, L. Ho, and Y. Chiang, *Clin. Chem.* 39, 1659 (**1993**).
4. T. Matsuya, S. Tashiro, N. Hoshino, N. Shibata, Y. Nagasaki, and K. Kataoka, *Anal. Chem.* 75, 6124 (**2003**).
5. E. Vieira Neto, E. C. D. Carvalho, and A. Fonseca, *Clin. Chim. Acta* 360, 151 (**2005**).
6. T. O'Riordan, A. Soini, J. Soini, and D. Papkovsky, *Anal. Chem.* 74, 5845 (**2002**).
7. K. Matsumoto, J. Yuan, G. Wang, and H. Kimura, *Anal. Biochem.* 276, 81 (**1999**).
8. C. W. Babb, D. R. Coon, and G. A. Rechnitz, *Anal. Chem.* 67, 763 (**1995**).
9. J. Rife, M. Miller, P. Sheehan, C. Tamanaha, M. Tondra, and L. Whitman, *Sens. Actuators A Phys.* 107, 209 (**2003**).
10. S.-H. Chung, A. Hoffmann, K. Guslienko, S. Bader, C. Liu, B. Kay, L. Makowski, and L. Chen, *J. Appl. Phys.* 97, 10R101 (**2005**).
11. G. Li, S. Sun, R. J. Wilson, R. L. White, N. Pourmand, and S. X. Wang, *Sens. Actuators A Phys.* 126, 98 (**2006**).

12. F. Ludwig, S. Mauselein, E. Heim, and M. Schilling, *Rev. Sci. Instrum.* 76, 106102 (**2005**).
13. R. Kötitz, W. Weitschies, L. Trahms, and W. Semmler, *J. Magn. Magn. Mater.* 201, 102 (**1999**).
14. W. F. Brown, Jr, *Phys. Rev.* 130, 1677 (**1963**).
15. Y. Chemla, H. Grossman, Y. Poon, R. McDermott, R. Stevens, M. Alper, and J. Clarke, *Proceedings of the National Academy of Sciences* 97, 14268 (**2000**).
16. I. Koh and L. Josephson, *Sensors* 9, 8130 (**2009**).
17. F. Ludwig, E. Heim, and M. Schilling, Magnetorelaxometry of magnetic nanoparticles-a new method for the quantitative and specific analysis of biomolecules 2004, *4th IEEE Conference on Nanotechnology*, Munich, Germany, August (**2004**).
18. C. B. Kriz, K. Rådevik, and D. Kriz, *Anal. Chem.* 68, 1966 (**1996**).
19. K. D. Mahajan, G. B. Vieira, G. Ruan, B. L. Miller, M. B. Lustberg, J. J. Chalmers, R. Sooryakumar, and J. O. Winter, *Chem. Eng. Prog.* 108, 41 (**2012**).
20. A. Elias and A. Tsourkas, *ASH Education Program Book* 2009, 720 (**2009**).
21. P. C. Fannin, L. Cohen-Tannoudji, E. Bertrand, A. T. Giannitsis, C. Mac Oireachtaigh, and J. Bibette, *J. Magn. Magn. Mater.* 303, 147 (**2006**).
22. S. Chung, A. Hoffmann, S. Bader, C. Liu, B. Kay, L. Makowski, and L. Chen, *Appl. Phys. Lett.* 85, 2971 (**2004**).
23. P. C. Fannin, *J. Magn. Magn. Mater.* 252, 59 (**2002**).
24. G. Mihajlovic, P. Xiong, S. von Molnár, K. Ohtani, H. Ohno, M. Field, and G. J. Sullivan, *Appl. Phys. Lett.* 87, 112502 (**2005**).
25. L. Li, K. Mak, C. Leung, K. Chan, W. Chan, W. Zhong, and P. Pong, *IEEE Trans. Magn.* 48, 3299 (**2012**).
26. C. Gooneratne, I. Giouroudi, and J. Kosel, Microdevice with half-ring shaped GMR sensors for magnetic bead manipulation and detection, Advancement in Sensing Technology, Springer, Berlin Heidelberg (**2013**), p. 121.
27. S. X. Wang and G. Li, *IEEE Trans. Magn.* 44, 1687 (**2008**).
28. J. S. Beveridge, J. R. Stephens, and M. E. Williams, *Annu. Rev. Anal. Chem.* 4, 251 (**2011**).
29. R. Arbain, M. Othman, and S. Palaniandy, *Miner. Eng.* 24, 1 (**2011**).
30. S. Banerjee, S. Roy, J. Chen, and D. Chakravorty, *J. Magn. Magn. Mater.* 219, 45 (**2000**).
31. K. Wu, P. Kuo, Y. Yao, and E. Tsai, *IEEE Trans. Magn.* 37, 2651 (**2001**).
32. J. Lopez-Perez, M. Lopez-Quintela, J. Mira, and J. Rivas, *IEEE Trans. Magn.* 33, 4359 (**1997**).
33. W. Y. William, J. C. Falkner, C. T. Yavuz, and V. L. Colvin, *Chem. Comm.* 2306 (**2004**).
34. L. Shen, P. E. Laibinis, and T. A. Hatton, *Langmuir* 15, 447 (**1999**).
35. J.-P. Jolivet, É. Tronc, and C. Chanéac, *C. R. Chim.* 5, 659 (**2002**).
36. B. Sahoo, S. K. Sahu, and P. Pramanik, *J. Mol. Catal. B: Enzym.* 69, 95 (**2011**).
37. J.-H. Wu, S. P. Ko, H.-L. Liu, S. Kim, J.-S. Ju, and Y. K. Kim, *Matt. Lett.* 61, 3124 (**2007**).
38. L. A. Harris, J. D. Goff, A. Y. Carmichael, J. S. Riffle, J. J. Harburn, T. G. St. Pierre, and M. Saunders, *Chem. Mater.* 15, 1367 (**2003**).
39. K. Mandel, F. Hutter, C. Gellermann, and G. Sextl, *Colloid Surface A* 390, 173 (**2011**).
40. S. Wan, J. Huang, M. Guo, H. Zhang, Y. Cao, H. Yan, and K. Liu, *J. Biomed. Mater. Res. A* 80, 946 (**2007**).
41. J. Lu, S. Yang, K. M. Ng, C.-H. Su, C.-S. Yeh, Y.-N. Wu, and D.-B. Shieh, *Nanot.* 17, 5812 (**2006**).
42. M. Carmen Bautista, O. Bomati-Miguel, M. del Puerto Morales, C. J. Serna, and S. Veintemillas-Verdaguer, *J. Magn. Magn. Mater.* 293, 20 (**2005**).
43. L. Li, K. Y. Mak, J. Shi, C. H. Leung, C. M. Wong, C. W. Leung, C. S. K. Mak, N. M. M. Chan, S. B. Chan, W. Zhong, C. Shueh, K. W. Lin, and P. W. T. Pong, Synthesis, characterization, and *in vitro* biocompatibility assay of Fe_3O_4 nanoparticles, *Proceeding of IUMRS International conference in Asia (IUMRS-ICA 2011)*, Taipei, Taiwan, September (**2011**).
44. I. Capek, *Adv. Colloid Interface Sci.* 110, 49 (**2004**).
45. J. Vidal-Vidal, J. Rivas, and M. A. López-Quintela, *Colloid Surface A* 288, 44 (**2006**).
46. A. B. Chin and I. I. Yaacob, *J. Mater. Process. Tech.* 191, 235 (**2007**).
47. C. Okoli, M. Sanchez-Dominguez, M. Boutonnet, S. Järås, C. N. Civera, C. Solans, and G. R. Kuttuva, *Langmuir* 28, 8479 (**2012**).
48. A. K. Gupta and M. Gupta, *Biomater.* 26, 3995 (**2005**).
49. J. Xie, S. Peng, N. Brower, N. Pourmand, S. X. Wang, and S. Sun, *Pure Appl. Chem.* 78, 1003 (**2006**).
50. X. Teng and H. Yang, *J. Mater. Chem.* 14, 774 (**2004**).
51. J. Rockenberger, E. C. Scher, and A. P. Alivisatos, *J. Am. Chem. Soc.* 121, 11595 (**1999**).
52. S. Sun and H. Zeng, *J. Am. Chem. Soc.* 124, 8204 (**2002**).
53. K. Woo, J. Hong, S. Choi, H.-W. Lee, J.-P. Ahn, C. S. Kim, and S. W. Lee, *Chem. Mater.* 16, 2814 (**2004**).
54. M. Gonzales and K. M. Krishnan, *J. Magn. Magn. Mater.* 311, 59 (**2007**).
55. W. Y. William, E. Chang, C. M. Sayes, R. Drezek, and V. L. Colvin, *Nanot.* 17, 4483 (**2006**).
56. K. Simeonidis, S. Mourdikoudis, M. Moulla, I. Tsiaoussis, C. Martinez-Boubeta, M. Angelakeris, C. Dendrinou-Samara, and O. Kalogirou, *J. Magn. Magn. Mater.* 316, e1 (**2007**).
57. J. Rockenberger, E. C. Scher, and A. P. Alivisatos, *Journal of the American Chemical Society* 121, 11595 (**1999**).
58. Z. Li, Q. Sun, and M. Gao, *Angew. Chem. Int. Ed.* 44, 123 (**2005**).
59. A. Roca, M. Morales, K. O'Grady, and C. Serna, *Nanot.* 17, 2783 (**2006**).
60. G. Zhen, B. W. Muir, B. A. Moffat, P. Harbour, K. S. Murray, B. Moubaraki, K. Suzuki, I. Madsen, N. Agron-Olshina, L. Waddington, P. Mulvaney, and P. G. Hartley, *J. Phys. Chem. C* 115, 327 (**2010**).
61. H. Grossman, W. Myers, V. Vreeland, R. Bruehl, M. Alper, C. Bertozzi, and J. Clarke, *Proc. Natl. Acad. Sci.* 101, 129 (**2004**).
62. E. Heim, F. Ludwig, and M. Schilling, *J. Magn. Magn. Mater.* 321, 1628 (**2009**).
63. F. Ludwig, E. Heim, S. Mäuselein, D. Eberbeck, and M. Schilling, *J. Magn. Magn. Mater.* 293, 690 (**2005**).
64. P. Ripka, *Sens. Actuators A Phys.* 106, 8 (**2003**).
65. S.-J. Han and S. Wang, *J. Lab. Autom.* 15, 93 (**2010**).
66. A. K. Bhuiya, T. Mitake, M. Asai, T. Ito, S. Chosakabe, T. Yoshida, K. Enpuku, and A. Kandori, *IEEE Trans. Magn.* 47, 2867 (**2011**).
67. A. K. Bhuiya, M. Asai, H. Watanabe, T. Hirata, Y. Higuchi, T. Yoshida, and K. Enpuku, *IEEE Trans. Magn.* 48, 2838 (**2012**).
68. F. Ibraimi, K. Kriz, H. Merin, and D. Kriz, *J. Magn. Magn. Mater.* 321, 1632 (**2009**).
69. J. Connolly and T. G. St. Pierre, *J. Magn. Magn. Mater.* 225, 156 (**2001**).
70. K. Park, T. Harrah, E. B. Goldberg, R. P. Guertin, and S. Sonkusale, *Nanot.* 22, 085501 (**2011**).
71. R. Del Real, G. Rosa, and H. Guerrero, *Rev. Sci. Instrum.* 75, 2351 (**2004**).
72. A. Ranzoni, G. Sabatte, L. J. van Ijzendoorn, and M. W. J. Prins, *ACS Nano* 6, 3134 (**2012**).
73. A. Ranzoni, J. J. H. B. Schleipen, L. J. van Ijzendoorn, and M. W. J. Prins, *Nano Lett.* 11, 2017 (**2011**).
74. K. Enpuku, Y. Tamai, T. Mitake, T. Yoshida, and M. Matsuo, *J. Appl. Phys.* 108, 034701 (**2010**).
75. L. Hy and Q. Sj, A study on human magnetocardiogram using giant magnetoimedance sensor, *Proceedings of the 2012 International Conference on Electronics, Communications and Control*, Zhoushan, China, October (**2012**).
76. J. Lenz and S. Edelstein, *IEEE Sens. J.* 6, 631 (**2006**).
77. A. Jander, C. Smith, and R. Schneider, *Nondestructive Evaulation for Health Monitoring and Diagnostics* 1 (**2005**).

78. D. R. Baselt, G. U. Lee, M. Natesan, S. W. Metzger, P. E. Sheehan, and R. J. Colton, *Biosens. Bioelectron.* 13, 731 **(1998)**.

79. S. J. Osterfeld, H. Yu, R. S. Gaster, S. Caramuta, L. Xu, S.-J. Han, D. A. Hall, R. J. Wilson, S. Sun, and R. L. White, *Proc. Natl. Acad. Sci.* 105, 20637 **(2008)**.

80. A. C. Mak, S. J. Osterfeld, H. Yu, S. X. Wang, R. W. Davis, O. A. Jejelowo, and N. Pourmand, *Biosens. Bioelectron.* 25, 1635 **(2010)**.

81. R. S. Gaster, L. Xu, S.-J. Han, R. J. Wilson, D. A. Hall, S. J. Osterfeld, H. Yu, and S. X. Wang, *Nat. Nanotechnol.* 6, 314 **(2011)**.

82. W. Shen, B. D. Schrag, M. J. Carter, J. Xie, C. Xu, S. Sun, and G. Xiao, *J. Appl. Phys.* 103, 07A306 **(2008)**.

83. W. Shen, B. D. Schrag, M. J. Carter, and G. Xiao, *Appl. Phys. Lett.* 93, 033903 **(2008)**.

84. Z. Lei, L. Li, G. Li, C. Leung, J. Shi, C. Wong, K. Lo, W. Chan, C. Mak, and S. Chan, *J. Appl. Phys.* 111, 07E505 **(2012)**.

85. H. Chiriac, M. Tibu, A.-E. Moga, and D. D. Herea, *J. Magn. Magn. Mater.* 293, 671 **(2005)**.

86. L. Chen, C.-C. Bao, H. Yang, D. Li, C. Lei, T. Wang, H.-Y. Hu, M. He, Y. Zhou, and D.-X. Cui, *Biosens. Bioelectron.* 26, 3246 **(2011)**.

87. M.-H. Phan and H.-X. Peng, *Prog. Mater. Sci.* 53, 323 **(2008)**.

88. A. Kumar, S. Mohapatra, V. Fal-Miyar, A. Cerdeira, J. A. Garcia, H. Srikanth, J. Gass, and G. V. Kurlyandskaya, *Appl. Phys. Lett.* 91, 143902 **(2007)**.

89. M. Strömberg, J. Göransson, K. Gunnarsson, M. Nilsson, P. Svedlindh, and M. Strømme, *Nano Lett.* 8, 816 **(2008)**.

90. R. S. Gaster, D. A. Hall, C. H. Nielsen, S. J. Osterfeld, H. Yu, K. E. Mach, R. J. Wilson, B. Murmann, J. C. Liao, and S. S. Gambhir, *Nat. Med.* 15, 1327 **(2009)**.

91. S. J. Osterfeld, H. Yu, R. S. Gaster, S. Caramuta, L. Xu, S. J. Han, D. A. Hall, R. J. Wilson, S. Sun, and R. L. White, *Proc. Natl. Acad. Sci.* 105, 20637 **(2008)**.

92. L. Xu, H. Yu, M. S. Akhras, S. J. Han, S. Osterfeld, R. L. White, N. Pourmand, and S. X. Wang, *Biosens. Bioelectron.* 24, 99 **(2008)**.

Received: 12 July 2013. Accepted: 1 September 2013.

REVIEW